CRediT author statement:

Pei Chen: Methodology, Validation, Formal Analysis, Investigation. **Fengwei Xie:** Conceptualization, Methodology, Validation, Formal analysis, Investigation, Resources, Data Curation, Writing - Original Draft, Writing - Review & Editing, Visualization, Supervision, Project administration, Funding acquisition. **Fengzai Tang:** Investigation, Writing - Original Draft. **Tony McNally:** Conceptualization, Resources, Writing - Review & Editing, Supervision, Funding acquisition.

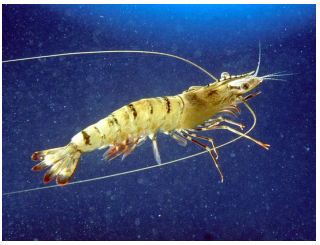

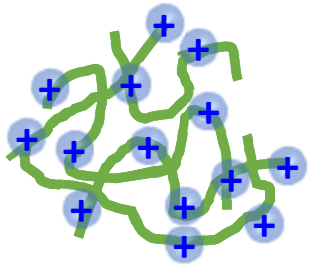

Chitosan

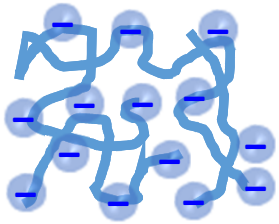

Carboxymethyl cellulose (CMC)

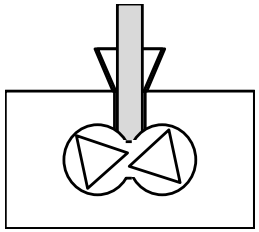

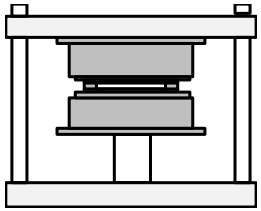

Chitosan film

Hydrated

Chitosan/CMC film

Hydrated

Thermomechanical-induced polyelectrolyte complexation between chitosan and carboxymethyl cellulose enabling unexpected hydrolytic stability‡

Pei Chen [a,b], Fengwei Xie [b,c,*,†], Fengzai Tang [d], Tony McNally [b,**]

[a] *College of Food Science, South China Agricultural University, Guangzhou, Guangdong 510642, China*

[b] *International Institute for Nanocomposites Manufacturing (IINM), WMG, University of Warwick, Coventry CV4 7AL, United Kingdom*

[c] *School of Chemical Engineering, The University of Queensland, Brisbane, Qld 4072, Australia*

[d] *WMG, University of Warwick, Coventry CV4 7AL, United Kingdom*

[*] Corresponding author. Email addresses: d.xie.2@warwick.ac.uk, fwhsieh@gmail.com (F. Xie)

[**] Corresponding author. Email address: t.mcnally@warwick.ac.uk (T. McNally)

[†] This author leads the research.

‡ Supplementary material is provided.

Abstract

Natural biopolymers such as chitosan and cellulose have demonstrated huge potential in important and rapidly growing environmental and biomedical applications. However, it is always challenging to create advanced functional biopolymer materials with enhanced hydrolytic stability cost-effectively. Here, we report an advance in preparing biopolymer polyelectrolyte complexed materials based on chitosan and carboxymethyl cellulose (CMC) using a “dry”, thermo-mechanical kneading method. Despite the high hydrophilicity of chitosan and CMC, the resulting films showed excellent dimensional stability and structural integrity (27% dimensional expansion and 94% weight

increase after hydration for one day). In comparison, chitosan-only films were swollen dramatically under the same conditions, with a 138% dimensional expansion and a 913% rise in weight, which were also fragile. We propose that our processing method led to polyelectrolyte complexation between chitosan and CMC generating physical crosslinking points in the materials, which stabilised the films in water. Interestingly, the greater hydrolytic stability of chitosan/CMC films is in contrast with their higher surface hydrophilicity, a contribution from CMC. Our simple approach to engineering high-performance biopolymer materials without resorting to complex chemistries can be envisioned to bring about a new direction in the design of advanced functional materials where sustainability and cost-effectiveness are priorities.

Keywords: A. Biocomposites; A. Nanocomposites; A. Polymer-matrix composites (PMCs); Biopolymer

1 Introduction

In recent years, there has been huge interest in using natural biopolymers for materials development due to the desire to achieve sustainability and to make use of the unique properties of these naturally occurring organic compounds. Natural biopolymers such as cellulose, chitin, proteins, and starch have many advantages over traditional synthetic polymers such as wide availability, renewability, nontoxicity, biocompatibility, and biodegradability. Moreover, their unique characteristics could find potential use in value-added applications such as antimicrobial biomaterial coatings [1], antifouling oil/water separation meshes [2, 3], tribological power generation [4], smart textiles and soft robotics [5], and patches for the treatment of heart disease [6].

On the other hand, polyelectrolyte complexation has been an interesting topic as it opens the

possibility of creating responsive and smart material systems with tailored strength or texture based on the dissociation/reassociation of oppositely charged polymer chains [7, 8]. This is also an important approach to creating polysaccharide-based micro- and nanoparticles, beads, capsules, and hydrogels with desired structures (e.g., core-shell) and functional properties for drug delivery, wound dressing, tissue engineering, and other fields [9-11]. In particular, chitosan (derived from chitin by deacetylation), as a cationic polysaccharide, can be complexed with negatively charged biopolymers such as proteins, alginate, carboxymethyl starch, pectin, chondroitin sulphate, and dextrin sulphate [12]. However, research on polysaccharide-based polyelectrolyte-complexed films has just started. Chitosan/gum Arabic complexed films have been shown to exhibit suitable mechanical and functional properties (antimicrobial and controlled-release) for food packaging [13] and drug delivery [14]. Basu et al. [15] demonstrated the excellent oil and water barrier properties of chitosan/carboxymethyl cellulose (CMC) polyelectrolyte complexed films.

While studies on biopolymer materials (including polyelectrolyte complexes) have predominantly relied on solution processing methods, thermomechanical processing has been shown to be sustainable and cost-effective for the processing biopolymers (e.g., chitosan [16, 17] and alginate [18]). Any processing of biopolymers should be able to effectively disrupt the hydrogen bonding networks and provide a route to re-establish new hydrogen bonds in the post-processed materials. In this work, we report the preparation of chitosan/CMC polyelectrolyte complexed films using a thermomechanical processing method, which has not been attempted before. The hybridisation of CMC as a much cheaper biopolymer with chitosan is expected to reduce the cost of the resulting materials. Whilst the hybridisation of chitosan and cellulose normally relies on

hydrogen bonding between the two phases to achieve property enhancement [19, 20], our work here indicates additional polyelectrolyte complexation between chitosan and CMC. Without chemical reaction, our engineered films unexpectedly show much better hydrolytic stability than chitosan or CMC alone. Thus, the materials developed could be significant potential for biomedical applications such as tissue engineering and wound healing. Furthermore, we tailored the material properties by incorporating two naturally-occurring nanoclays (montmorillonite, MMT, in the form of two-dimensional (2D) nanoplatelets; and sepiolite, SPT, in the form of one-dimensional (1D) nanoneedles) in the formulations. As these nanoclays are negatively charged in their natural forms due to isomorphic substitutions occurring inside the clay platelets [21, 22], the competing interactions among chitosan, CMC and nanoclay could be interrogated. Therefore, our work could provide fundamental insights into the rational design of multifunctional multiphasic biopolymer nanocomposites with tailored structures and properties for even wider applications.

2 Experimental Section

2.1 Materials

A low-molecular-weight chitosan was used in this work, which is commercially available and described previously [23]. This chitosan has been characterised in our previous study [24]. Carboxymethyl cellulose (CMC) sodium, with a molecular mass of 90,000 $g \cdot mol^{-1}$, a degree of substitution (DS) of 0.7, and a viscosity of 50–100 mPa·s (Brookfield, 2% solution, at 25 °C), was purchased from Shanghai Macklin Biochemical Co., Ltd., Shanghai, China. The characteristics of the CMC are shown in Figure S1. The details of other materials and chemicals are given in our previous report [24].

2.2 Sample preparation

A range of biopolymer samples were prepared with their formulations and codes shown in Table 1. Montmorillonite (MMT) or sepiolite (SPT) was dispersed in 25 mL of 2M formic acid in small vials, which were treated with ultrasound using a tip-type sonicator (200 W, 24 kHz) for 10 min. Chitosan and/or CMC were pre-blended mechanically for 20 min, during which 2M formic acid solution (90 mL) and the treated nanoclay suspension (25 mL) were added dropwise. Then, the pre-blended mixtures were stored hermetically overnight in a fridge before thermo-mechanical mixing and compression moulding. In Table 1, codes such as "A/M-F" and "B/S-F" are used, where "A" is the matrix with only chitosan while "B" indicates chitosan/CMC was the matrix; "M" (MMT), "S" (SPT), or "MS" (MMT and SPT) represents the clay used; and "F" means processed as a film.

Table 1. Sample codes and compositions.

Sample	Chitosan (g)	CMC (g)	MMT (g)	SPT (g)	2M Formic acid (mL)
A-F	45	–	–	–	90+25
A/M-F	45	–	0.6750 (1.5%)	–	90+25
A/S-F	45	–	–	0.6750 (1.5%)	90+25
A/MS-F	45	–	0.3375 (0.75%)	0.3375 (0.75%)	90+25
B-F	22.5	22.5	–	–	90+25
B/M-F	22.5	22.5	0.6750 (1.5%)	–	90+25
B/S-F	22.5	22.5	–	0.6750 (1.5%)	90+25
B/MS-F	22.5	22.5	0.3375 (0.75%)	0.3375 (0.75%)	90+25

The thermo-mechanical mixing was carried out for 15 min at a screw speed of 30 rpm and a

temperature of 80 °C using a HAAKE™ Rheomix OS Lab Mixer (Thermo Fisher Scientific, Waltham, MA, USA). The thermally processed materials were compression-moulded into films of 1.2 mm thickness using a COLLIN® P200 P/M platen press (COLLIN Lab & Pilot Solutions GmbH, Ebersberg, Germany). The mould used has an interior platen size of 150 mm ×150 mm and a thickness of 1.2 mm. The conditions used for hot pressing were firstly, the sample was held at 110 °C and 160 bar for 10 min, followed by cooling to, and maintained at, room temperature (RT) for another 5 min. The compression-moulded films were stored in desiccators maintained at 57% relative humidity (RH) achieved using saturated NaBr for 3 weeks before characterisation. In the desiccators, toluene was placed in an open beaker to prevent the samples from becoming mouldy. After conditioning, Type V dumbbell-shaped specimens were cut from the sheets according to ASTM Standard D638-14, which were then left openly at RT for 2 days before characterisation.

3 Results and Discussion

3.1 Hydrolytic stability and mechanical properties

By simply thermomechanical mixing of a biopolymer with limited amounts of aqueous acid followed by compression moulding, we obtained well-formed biopolymer films (Figure S2). Chitosan (A) films were light brown whilst the chitosan/CMC (B) formulations had a darker colour, especially with the addition of nanoclay. When the films were prepared, they were flexible (particularly, chitosan/CMC films were softer) but, they all became rigid with similar density (Figure S3) after conditioning (i.e. a process for removal of excess moisture and for recrystallisation). However, after soaking in water for up to 24 h, the conditioned chitosan films were swollen dramatically (Figure S2 and Figure S4). Specifically, the dimensions (widths) of A-F at 30 min and 1

day were 184±19% and 238±25%, respectively, of its original dimension; the weights of A-F at 30 min and 1 day were 357±41% and 1013±29%, respectively, of its original weight. The addition of nanoclay could only moderately reduce the dimensional and weight changes. In contrast, although the conditioned chitosan/CMC (B) films still swelled in water, they were much more hydrolytically stable (Figure S2 and Figure S4). This is unexpected considering that a low-molecular-mass chitosan and a CMC sodium salt were used, which are rather hydrophilic or even water-soluble. Even after hydration for 1 day, the B-F film had a 127±1% increase in dimensions and was 194±2% weight of its original value, both much lower than the percentages for the chitosan (A) films. These changes were only reduced marginally by the addition of nanoclay. For example, the dimension and weight of B/MS-F at 1 day were 121±2% and 176±0% of its original values. The enhanced hydrolytic stability could make this new type of polysaccharide complexed material highly useful for application as artificial skin and in wound dressings. The increased resistance to swelling with water can be attributed to the strong hydrogen-bonding and electrostatic interactions formed between the two reversely charged polysaccharides during processing. The complexation may have contributed to the formation of physical crosslinks between the materials, which could stabilise the polyelectrolyte complexed films in water.

We tested the tensile properties of the biopolymer films both in the dry state (after conditioning) and in a wet state after soaking in water for 30 min (Figure 1). The mechanical properties of these different formulations in the dry state were similar, except that chitosan/CMC (B) films displayed slightly higher σ_t, and lower ε_b, especially with the addition of nanoclay. All the films had quite small elongation at break (ε_b) values (up to 22.6%), indicating their brittle character. Therefore, we

consider the mechanical properties of these dry samples were mainly determined by the hydrogen bonding between the biopolymer chains. Correspondingly, recent research has shown that with enhanced hydrogen bonding between cellulose molecular chains, densified bulk natural wood could display remarkably increased mechanical properties and enhanced dimensional stability [25, 26]. For the dry films, the stress–strain curve is typical of a hard and tough polymer, with strain hardening observed (Figure S5a), which verifies the strong interactions between biopolymer chains.

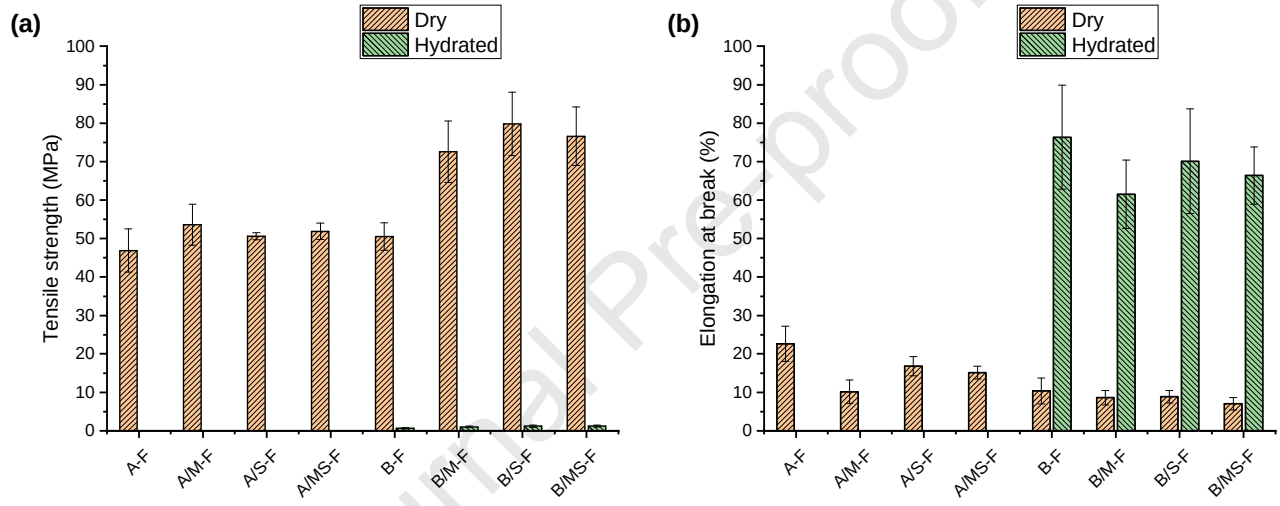

Figure 1. Tensile mechanical properties a) tensile strength and b) elongation at break of chitosan films in the dry state and chitosan/CMC films both in the dry state and in a hydrated state after soaking in water for 30 min. The error bars represent standard deviations.

Compared to the dry samples, hydrated chitosan/CMC (B) films showed significantly reduced tensile strength (σ_t) and remarkably higher ε_b. Regarding this, the hydrogen bonds might have been most disrupted by water molecules through interacting with biopolymer hydroxyl groups. However, there should be some physical crosslinking points resulting from polyelectrolyte complexation in the materials, which were responsible for maintaining the integrity and dimensional stability of the biopolymer films even after hydration. This loss of intra-/intermolecular hydrogen bonding can also

be observed from the linear tensile stress–strain curves (Figure S5b), which is typical of an elastomeric polymer. The chitosan/CMC polyelectrolyte complexed system here could be understood by making an analogy with polyurethane elastomers [27], whose elastomeric properties are governed by their crosslinks. On the contrary, for the chitosan (A) formulations, once the original hydrogen bonds were disrupted by water molecules, no other forces existed to maintain the confined molecular network and thus the whole material was dramatically swollen, which were even too delicate to have their mechanical properties tested.

3.2 Surface hydrophilicity

Contact angle (θ_c) was used to indicate the surface hydrophilicity of the different biopolymer films. As θ_c kept changing after a water drop was placed on the film surface, the values at 0 s and 60 s were recorded (Figure 2a). All chitosan (A) films displayed similar θ_c values at 0 s (90–96°) and at 60 s (65–72°) and the effect of nanoclay on the surface hydrophilicity was not apparent. Compared with chitosan (A) films, chitosan/CMC (B) films all had much lower θ_c values, indicating higher surface hydrophilicity (Figure 2b). In particular, B-F had θ_c of 71±6° at 0 s and 60±5° at 60 s. This is expected since CMC is a sodium salt having strong hydrophilicity and even water-dissolvable. Compared with B-F, B/M-F did not show any apparent difference in surface hydrophilic, whereas B/S-F and B/MS-F showed slightly higher θ_c values both at 0 s and 60 s. Although both nanoclays are hydrophilic, the more finely dispersed SPT (discussed in TEM section) may be more effective at shielding the interactions of biopolymer chains with water molecules, leading to increased surface hydrophobicity.

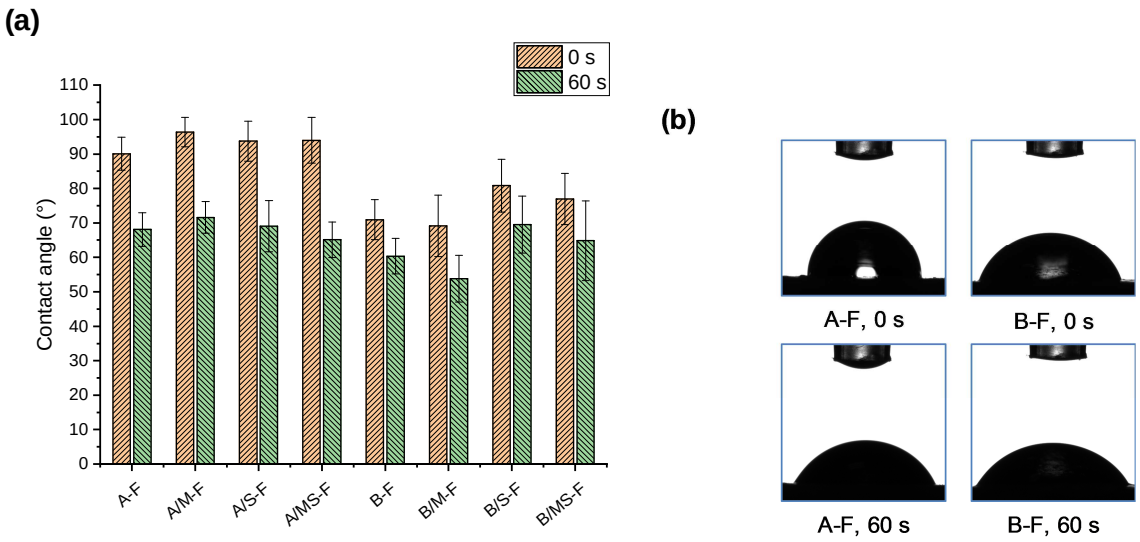

Figure 2. a) Contact angle values for different biopolymer films at 0 s and 60 s. The error bars represent standard deviations. b) Droplet images of A-F and B-F at 0 s and 60 s.

3.3 Morphology

Figure 3 shows the scanning electron microscopy (SEM) images of the different biopolymer films. All the samples showed a cohesive cryo-fractured surface with the absence of the original clumpy features of chitosan [24] and CMC (Figure S1), indicating successful processing of the biopolymers.

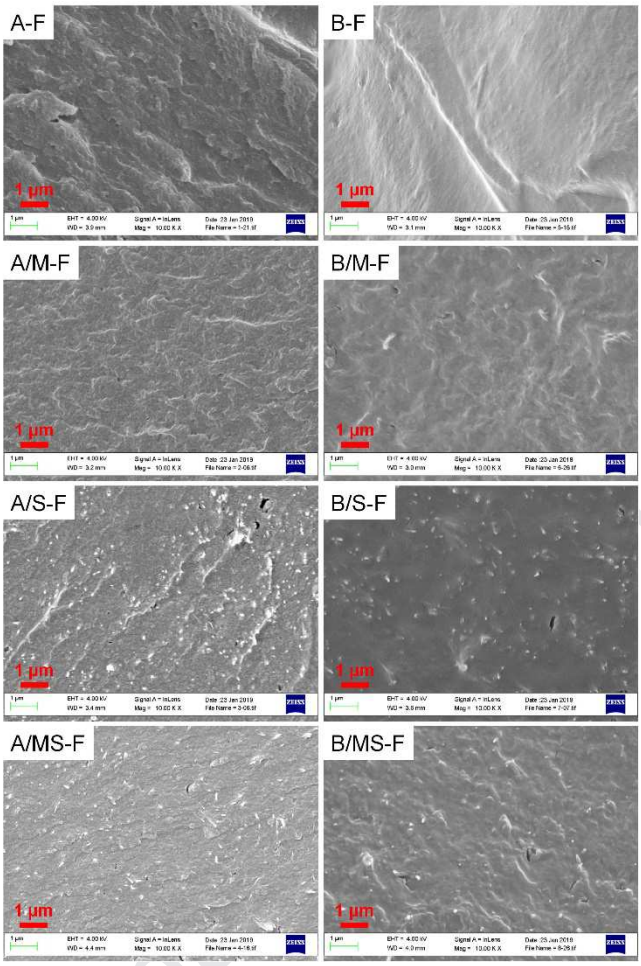

Figure 3. SEM images of the cryo-fractured surfaces of different biopolymers films.

Compared with that of A-F, the cryo-fractured surfaces of A/M-F, A/S-F, and A/MS-F appear more cohesive, most probably associated with the dispersed nanoclays. In contrast to chitosan (A) films, B-F signified a smoother cryo-fractured surface. However, this effect seemed to be negated by the addition of nanoclay. In particular, B/M-F and B/MS-F presented slightly uneven textures. In A/S-F, A/MS-F, B/S-F and B/MS-F, evenly dispersed white dots or even protruding rods were clearly noticeable. These features were the dispersed SPT nanoparticles, confirmed by STEM analysis below. Our SEM observations indicate that MMT had a greater effect than SPT on the morphology of the biopolymer films, which might be attributed to the larger surface area and thus stronger interactions of MMT.

194 While conventional transmission electron microscopy (TEM) analysis (Figure S6) shows some
195 large-sized features as nanoclay agglomerates [28] and biopolymer structures, such analysis in this
196 work, however, did not render a clear contrast of the dispersed fine particles within the matrix. Thus,
197 we employed scanning TEM (STEM) to acquire microscopic images of the different biopolymer
198 samples at higher magnifications with better resolutions. Figure 4 depicts MMT, SPT and MMT/SPT
199 particle distributions within chitosan (A) and chitosan/CMC (B) samples. For the sake of simplicity,
200 high-angle annular dark-field (HAADF) images taken at the same magnification are shown for each
201 of the samples, whilst a pair of high magnification HAADF and bright-field (BF) images are
202 presented for A/MS-F and B/MS-F.

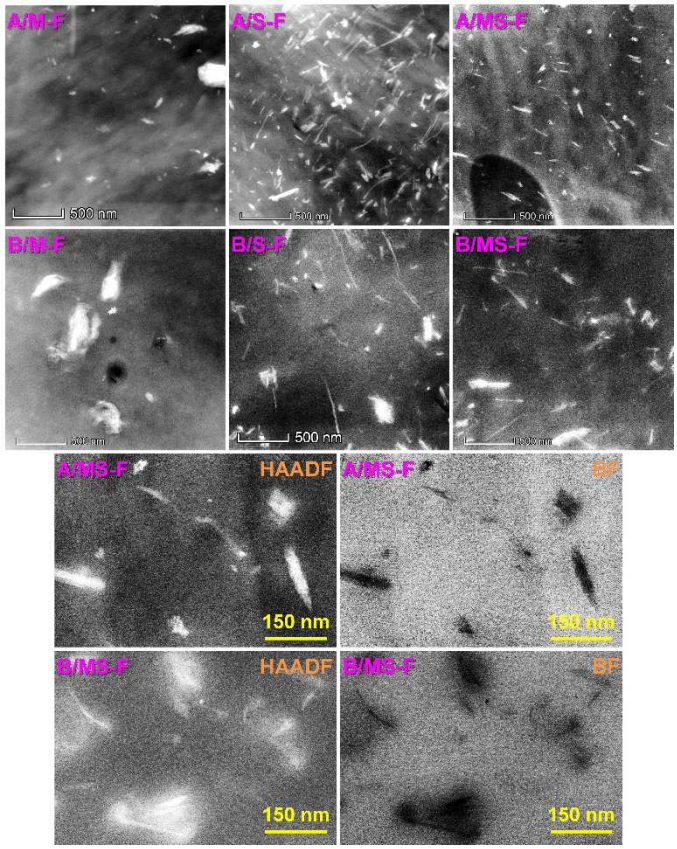

203

204 Figure 4. STEM images of different biopolymers films.

205 In A-F, MMT is present in a wide range of particle size distributions from < 50 nm to up to

206 400 nm with irregular shapes. In contrast but as expected, SPT particles in A/S-F appear needle-like
207 in shape, most of which are up to over 150 nm in length and with a large aspect ratio. A mixture of
208 MMT and SPT particles are clearly seen in A/MS-F, but both show a relatively smaller size
209 compared to when it was dispersed alone. The nanoclays (containing Si, Al, Mg, and K) in the
210 STEM images were different from the chitosan structural features (Figure S7) in morphology and
211 were also confirmed by energy-dispersive X-ray spectrometry (EDS) analysis, and the case of A/S-F
212 is given in Figure S8.

213 The B-F film shows a highly homogenous morphology without biopolymer structural features
214 (Figure S7), which could be due to the strong interactions between chitosan and CMC and the
215 possible plasticization effect of CMC on chitosan. For the chitosan/CMC (B) set of samples, the
216 distribution of MMT, SPT, and MMT/SPT are similar to that for the chitosan (A) samples. For both
217 A and B samples, there seem to be more MMT agglomerates than those of SPT, indicating stronger
218 inherent interactions between MMT platelets. The agglomerated and tactoid structures are formed by
219 ionic interactions between platelets and to some extent by the hydroxylated edge–edge interactions
220 of the silicate layers [28].

221 Irrespective of the type of clay, a finer dispersion of clay was found in chitosan alone (A) than in
222 chitosan/CMC (B) (see high magnification images). Both MMT and SPT are negatively charged and
223 have a hydrophilic character [21, 22, 29]. Chitosan, a polycation, could effectively interact with the
224 negatively charged clays, functioning as an organomodifier (surfactant) [21, 30]. Therefore, an
225 excellent dispersion of nanoclay in chitosan is expected. However, with CMC, a polyanion, in the
226 matrix, there could also be strong interactions between the two biopolymers, which weakened the

interactions between chitosan and nanoclay. In general, our processing protocol allowed an excellent dispersion of nanoclay in the biopolymer matrices for all samples.

3.4 Crystalline structure

Using X-ray diffraction (XRD), we examined the crystalline structures of the different biopolymer films (Figure 5). All chitosan (A) films showed similar XRD patterns, which are different from those of the unprocessed chitosan [24]. These films presented three major peaks at 2θ of about 13.5° ((020) reflection, *d*-spacing = 0.76 nm), 21.7° ((100) reflection, 0.48 nm), and 27.2° ((110) reflection, 0.38 nm). The (100) reflection shifted from 23.3° 2θ for the unprocessed chitosan to 21.7° 2θ for the processed chitosan (suggesting an enlarged *d*-spacing of the chitosan crystal lattice), while the (020) reflection of the unprocessed chitosan at 12.0° 2θ became extremely weak. The (100) and (020) reflections and the new (110) reflection are all attributed to the regular crystal lattice of chitosan [31], which were also observed previously for thermomechanically-processed chitosan films [16, 17, 23, 24, 32]. Moreover, the chitosan (A) formulations additionally showed some smaller peaks at 2θ of 10.0° (1.03 nm), 19.0° (0.54 nm), and 30.8° (0.34 nm). In this regard, the stronger acid treatment used in this work could have largely destroyed the original crystalline structure and a different crystalline structure formed during processing and conditioning. In this sense, the chitosan structural features observed under STEM (Figure S7) could be mainly due to recrystallisation.

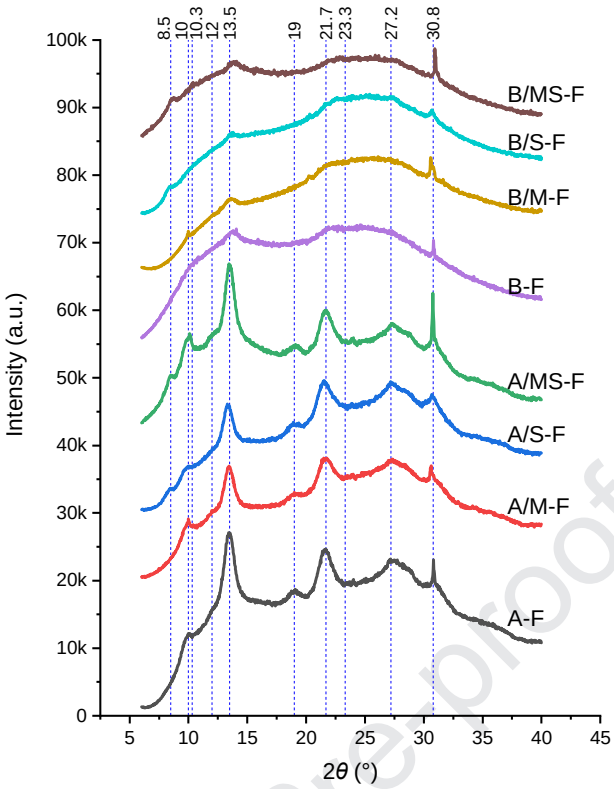

Figure 5. XRD patterns for different biopolymer films.

For A/MMT-F, the characteristic (001) refection of MMT was not shown, suggesting the successful delamination or partial exfoliation of MMT nanoplatelets. For A/S-F and A/MS-F, the characteristic SPT peak at 8.5° 2θ is still observed, which is associated with the non-swelling nature of SPT (i.e. the zeolitic pores could not be affected by processing).

In contrast to chitosan (A) formulations, all chitosan/CMC (B) films showed mostly amorphous XRD patterns. The addition of CMC to the matrix largely suppressed the diffraction peaks characteristic of chitosan, with only the reflections at 13.5° and 30.8° 2θ remaining visible. The electrostatic and hydrogen bonding interactions between chitosan and CMC could have limited the recrystallisation of chitosan. Moreover, the original structure of CMC should have also been destroyed by processing as its characteristic peak at 23.3° (d-spacing = 0.44 nm) (Figure S1b), ascribed to the (110) lattice plane of the cellulose II crystalline structure [33-36], was not visible for

chitosan/CMC films.

From the XRD results, the crystalline structure of the films was mainly influenced by the biopolymers whereas inclusion of nanoclays had no major effect.

3.5 Molecular Interactions

Fourier-transform infrared (FTIR) analysis was undertaken to understand the chemical interactions in the different biopolymer films (Figure 6). Chitosan (A) films displayed quite similar FTIR spectra, which were close to that of the unprocessed chitosan [24], This suggests no significant molecular interactions occurred resulting from processing or the addition of nanoclays.

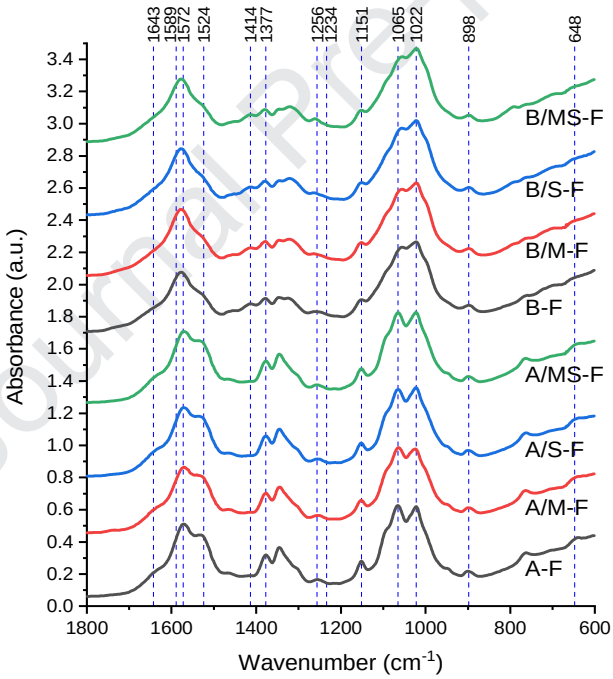

Figure 6. FTIR spectra for different biopolymer films.

Chitosan/CMC (B) films had FTIR spectra that were largely similar to those of chitosan (A) formulations. Original CMC displays characteristic bands at 1055 cm^{-1}, 1414 cm^{-1}, and 1589 cm^{-1} (Figure S1c) for the C─O stretching vibration band of ether groups and the asymmetric and symmetric modes of stretching vibrations of carboxylate ions, respectively [37-40]. In the complexed

films, the characteristic peak of CMC at 1414 cm^{-1} was weak and those of CMC at 1055 cm^{-1} and 1589 cm^{-1} (Figure S1c) could be overlapped by the bands of chitosan and/or have shifted positions. Moreover, there were shifts in the positions of some characteristic bands of chitosan. The bands at 1572 cm^{-1} (amide II or the ─NH_2 group of chitosan), 1256 cm^{-1} (amide III), and 1377 cm^{-1} (the CH_3 symmetrical deformation mode) were blue-shifted, while that at 1056 cm^{-1} (the skeletal vibration of glucosamine involving the ─C─O─ stretching) was red-shifted. These shifts indicate strong molecular interactions between chitosan and CMC involving the saccharide backbone, amine and amide groups of chitosan, and the carboxylate of CMC. On the other hand, the FTIR spectra of four chitosan/CMC formulations appear quite similar, suggesting that the addition of nanoclays did not change the biopolymer molecular interactions significantly.

3.6 Nanoindentation

Hardness (H) and reduced elastic modulus (E_r) on the nanoscale of the biopolymer samples were obtained from nanoindentation measurements (Figure 7). A constant indention depth of 2 µm was set for all samples as this was within the range that was free of the surface and substrate effects (Figure S9) [41]. Typical indentation loading-holding-unloading curves are shown in Figure 7a. For all the samples, the unloading curve inflects especially towards the end, reflecting the viscoelasticity of polymers [42]. The corresponding loads to the 2µm depth into the sample surface were higher for chitosan/CMC (B) formulations than for chitosan (A) formulations. The difference can be further examined using H (which is the result of the maximum load divided by the residual indentation area) (Figure 7b). Overall, polyelectrolyte complexation between the two biopolymers led to higher H, whereas the effect of nanoclay was minor. While a different measurement, this trend was in

agreement with Shore D bulk hardness results (Figure S10). Compared with A-F and A/M-F, A/S-F and A/MS-F displayed higher E_r values, which can be attributed to the needle-like nanoclay. However, a similar effect on addition of the nanoparticles was not observed for the chitosan/CMC formulations as they showed equivalent E_r. Again, the interactions between chitosan and CMC weakened the interactions between chitosan and nanoclay.

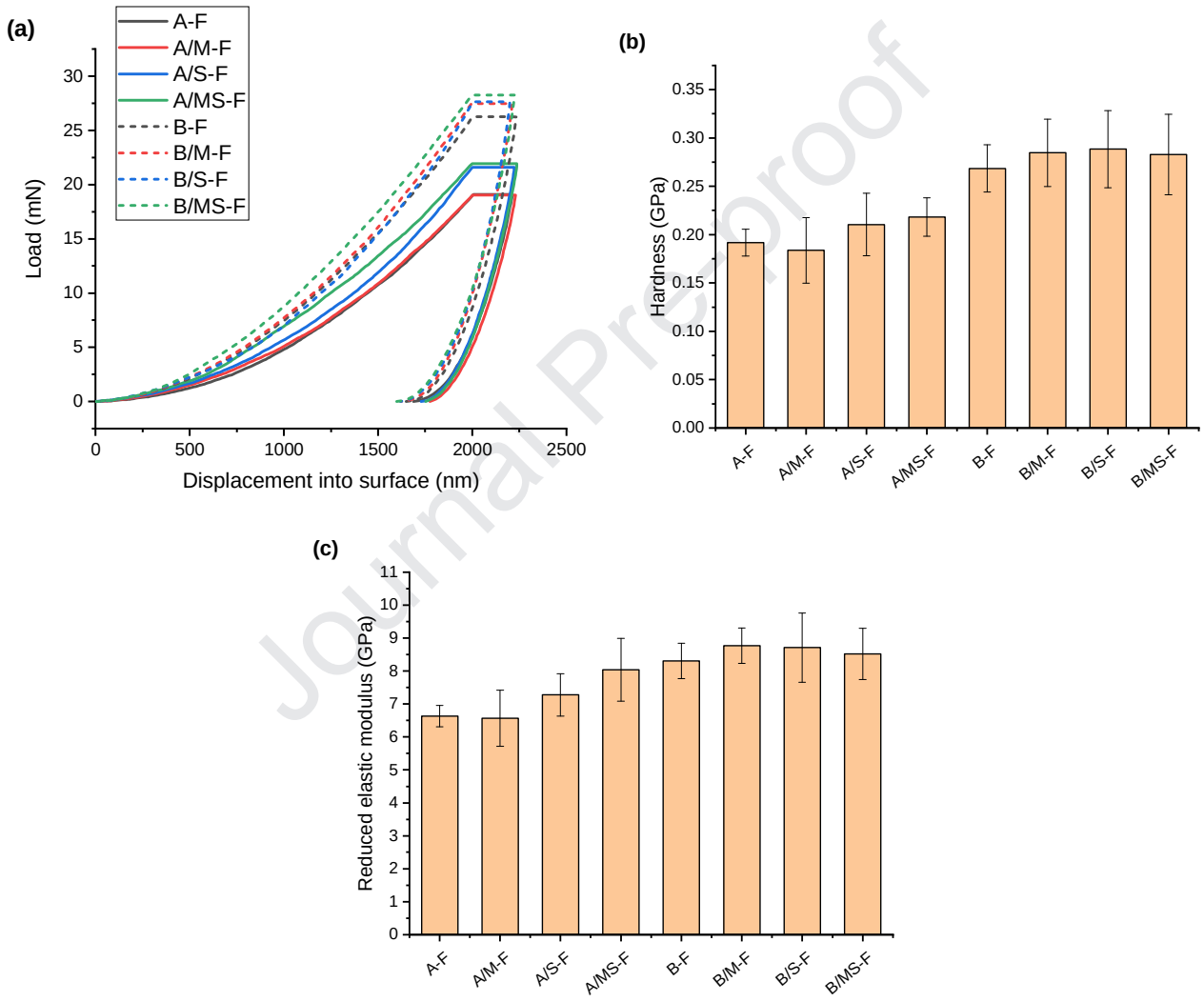

Figure 7. Typical loading-holding-unloading curves (a), hardness (b), and reduced modulus (c) of different biopolymer films. The error bars represent standard deviations.

3.7 Relaxation

Dynamic mechanical thermal analysis (DMTA) was used to investigate the molecular

304 relaxations of the biopolymer films (Figure 8). All chitosan (A) films exhibited very similar tan δ
305 profiles, with two transitions clearly identified. The weak transition centred at about −47 °C is
306 considered to be a β-relaxation attributed to the motions of the side chains or lateral groups of
307 chitosan interacting with small molecules such as water by hydrogen bonding [17, 43, 44]. A more
308 prominent transition with a peak temperature at about 119 °C may be associated with the α-transition
309 of chitosan. According to Quijada-Garrido et al. [43, 44], the α-relaxation can be attributed to the
310 glass transition and interpreted as torsional oscillations between two glucopyranose rings across a
311 glucosidic oxygen and the reordering of cooperative hydrogen bonds.

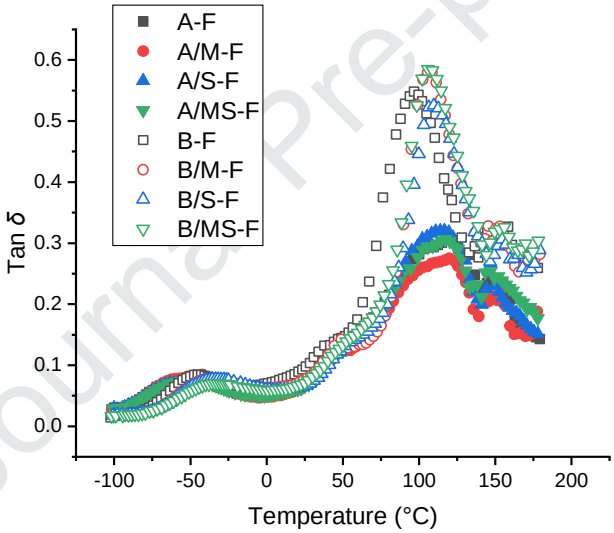

312
313 Figure 8. DMTA curves for different biopolymer films.

314 All chitosan/CMC (B) films displayed tan δ profiles similar to those of chitosan (A) films.
315 However, for B/M-F, B/S-F and B/MS-F, the β-relaxation moved to higher temperatures (centred at
316 *ca.* −37 °C), suggesting that the motions of the side chains or lateral groups of biopolymers were
317 more restricted due to the complexation of the two biopolymers. Compared with chitosan (A) films,
318 B-F had a lower glass transition temperature (T_g) of 96 °C and much higher peak intensity, indicating
319 CMC had a plasticisation effect on chitosan and made the system have more viscous behaviour (less

elastic behaviour). The addition of nanoclay resulted in an increase in the T_g of B-F to 107–110 °C for B/M-F, B/S-F, and B/MS-F. The inclusion of the nanoclay disrupts the interactions between chitosan and CMC.

Frequency scans from 0.01 Hz to 20 Hz of these biopolymer films at RT were also performed (Figure S11). For all the samples, E' kept increasing with frequency, corresponding to the viscoelasticity of polymers. Similar slopes of the E' versus frequency curves were shown on a log-log plot, implying that the nanoclays had no significant effect on the viscoelasticity of the samples.

3.8 Thermal stability

The thermal stability of the different biopolymer films was studied by TGA, with the derivative weight plots as a function of temperature shown in Figure 9. For all the chitosan (A) films, there was a major weight loss between 200 °C and 400 °C with the peak temperature unchanged even with the addition of nanoclay. Immediately before the major peak, there was a small, sharp peak centred between about 200 °C and 240 °C, attributed to the initial de-polymerisation of the biopolymer.

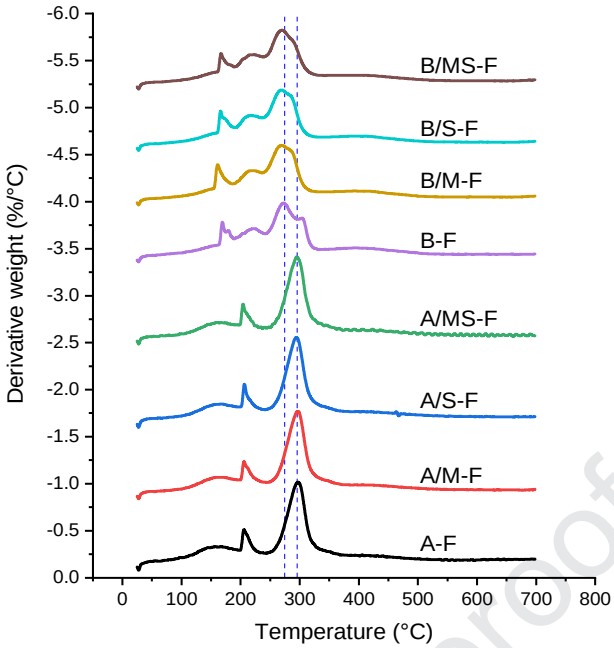

Figure 9. Derivative weight loss curves for different biopolymer films.

B-F showed major weight loss peaks associated with chitosan at 304 °C and CMC at 273 °C (the peak temperature of the original CMC was at 274 °C, see Figure S1). Furthermore, there were two small peaks at 169 °C and 223 °C, which could be ascribed to the initial de-polymerisation of the biopolymers. Apparently, the complexation with CMC made chitosan more prone to thermal degradation as the initial de-polymerisation occurred at lower temperatures. Regarding this, the Na^+ ion of CMC may have a sensitization effect on the thermal decomposition of chitosan. With the addition of nanoclay, all the derivative-weight peaks slightly shifted to lower temperatures. For example, for B/M-F, B/S-F, and B/MS-F, the CMC peak was all at 270 °C. This decreased thermal stability may be due to the sensitization effect of metal ions of the clays.

4 Conclusions

It has been demonstrated that hydrolytically stable chitosan/CMC polyelectrolyte complexed materials can be prepared by a method involving high-viscosity thermomechanical processing

enabling effective electrostatic complexation and hydrogen bonding between the two polysaccharides. This is so despite inclusion of the CMC in the matrix increasing the surface hydrophilicity of the blend material. As these biopolymer films contained no covalent crosslinks, the enhanced hydrolytic stability is totally unexpected and unconventional. Moreover, we propose the property changes caused by addition of MMT or SPT should be related to the competing interactions between chitosan, CMC and nanoclay and how these nanoparticles vary such highly-hydrogen-bonded biopolymer systems.

The novel biopolymer polyelectrolyte complexed materials developed in this study, without chemical reactions, will be highly beneficial especially for biomedical applications requiring excellent biocompatibility, biosafety, biodegradability, antimicrobial and antifungal activity where exceptional hydrolytic stability during in-service use is also demanding (e.g. in implants, antimicrobial wound healing, tissue engineering scaffolds, drug delivery carriers).

Conflicts of Interests

Declarations of interest: none

Acknowledgements

The authors acknowledge funding from the European Union's Horizon 2020 research and innovation programme under the Marie Skłodowska-Curie grant agreement No. 798225. P. Chen acknowledges the financial support from the China Scholarship Council (CSC) for her visiting position and thanks IINM, WMG, University of Warwick, UK for hosting her research visit. F. Xie also acknowledges support from the Guangxi Key Laboratory of Polysaccharide Materials and Modification, Guangxi University for Nationalities, China (Grant No. GXPSMM18ZD-02).

References

[1] G. Cado, R. Aslam, L. Séon, T. Garnier, R. Fabre, A. Parat, A. Chassepot, J.C. Voegel, B. Senger, F. Schneider, Y. Frère, L. Jierry, P. Schaaf, H. Kerdjoudj, M.H. Metz-Boutigue, F. Boulmedais, Self-Defensive Biomaterial Coating Against Bacteria and Yeasts: Polysaccharide Multilayer Film with Embedded Antimicrobial Peptide, Adv. Funct. Mater. 23(38) (2013) 4801-4809.

[2] J.J. Koh, G.J.H. Lim, X. Zhou, X. Zhang, J. Ding, C. He, 3D-Printed Anti-Fouling Cellulose Mesh for Highly Efficient Oil/Water Separation Applications, ACS Appl. Mater. Interfaces 11(14) (2019) 13787-13795.

[3] S. Zhang, F. Lu, L. Tao, N. Liu, C. Gao, L. Feng, Y. Wei, Bio-inspired anti-oil-fouling chitosan-coated mesh for oil/water separation suitable for broad ph range and hyper-saline environments, ACS Appl. Mater. Interfaces 5(22) (2013) 11971-11976.

[4] R. Wang, S. Gao, Z. Yang, Y. Li, W. Chen, B. Wu, W. Wu, Engineered and Laser‐Processed Chitosan Biopolymers for Sustainable and Biodegradable Triboelectric Power Generation, Adv. Mater. 30(11) (2018) 1706267.

[5] T. Jia, Y. Wang, Y. Dou, Y. Li, M. Jung de Andrade, R. Wang, S. Fang, J. Li, Z. Yu, R. Qiao, Z. Liu, Y. Cheng, Y. Su, M. Minary-Jolandan, R.H. Baughman, D. Qian, Z. Liu, Moisture Sensitive Smart Yarns and Textiles from Self-Balanced Silk Fiber Muscles, Adv. Funct. Mater. 29(18) (2019) 1808241.

[6] X. Lin, Y. Liu, A. Bai, H. Cai, Y. Bai, W. Jiang, H. Yang, X. Wang, L. Yang, N. Sun, H. Gao, A viscoelastic adhesive epicardial patch for treating myocardial infarction, Nature Biomedical Engineering (2019).

390 [7] Q. Wang, J.B. Schlenoff, The Polyelectrolyte Complex/Coacervate Continuum, Macromolecules
391 47(9) (2014) 3108-3116.
392 [8] Y. Zhao, Y. Wu, L. Wang, M. Zhang, X. Chen, M. Liu, J. Fan, J. Liu, F. Zhou, Z. Wang,
393 Bio-inspired reversible underwater adhesive, Nat. Commun. 8(1) (2017) 2218.
394 [9] S.L. Turgeon, C. Schmitt, C. Sanchez, Protein–polysaccharide complexes and coacervates, Curr.
395 Opin. Colloid Interface Sci. 12(4) (2007) 166-178.
396 [10] Z. Liu, Y. Jiao, Y. Wang, C. Zhou, Z. Zhang, Polysaccharides-based nanoparticles as drug
397 delivery systems, Adv. Drug Delivery Rev. 60(15) (2008) 1650-1662.
398 [11] O.G. Jones, D.J. McClements, Recent progress in biopolymer nanoparticle and microparticle
399 formation by heat-treating electrostatic protein–polysaccharide complexes, Adv. Colloid Interface
400 Sci. 167(1) (2011) 49-62.
401 [12] M.A. Mateescu, P. Ispas-Szabo, E. Assaad, 4 - Chitosan-based polyelectrolyte complexes as
402 pharmaceutical excipients, in: M.A. Mateescu, P. Ispas-Szabo, E. Assaad (Eds.), Controlled Drug
403 Delivery, Woodhead Publishing2015, pp. 127-161.
404 [13] T. Xu, C. Gao, Y. Yang, X. Shen, M. Huang, S. Liu, X. Tang, Retention and release properties
405 of cinnamon essential oil in antimicrobial films based on chitosan and gum arabic, Food
406 Hydrocolloids 84 (2018) 84-92.
407 [14] R.-Y. Tsai, P.-W. Chen, T.-Y. Kuo, C.-M. Lin, D.-M. Wang, T.-Y. Hsien, H.-J. Hsieh,
408 Chitosan/pectin/gum Arabic polyelectrolyte complex: Process-dependent appearance, microstructure
409 analysis and its application, Carbohydr. Polym. 101 (2014) 752-759.

410 [15] S. Basu, A. Plucinski, J.M. Catchmark, Sustainable barrier materials based on polysaccharide
411 polyelectrolyte complexes, Green Chem. 19(17) (2017) 4080-4092.
412 [16] V. Epure, M. Griffon, E. Pollet, L. Avérous, Structure and properties of glycerol-plasticized
413 chitosan obtained by mechanical kneading, Carbohydr. Polym. 83(2) (2011) 947-952.
414 [17] D.F. Xie, V.P. Martino, P. Sangwan, C. Way, G.A. Cash, E. Pollet, K.M. Dean, P.J. Halley, L.
415 Avérous, Elaboration and properties of plasticised chitosan-based exfoliated nano-biocomposites,
416 Polymer 54(14) (2013) 3654-3662.
417 [18] C. Gao, E. Pollet, L. Avérous, Properties of glycerol-plasticized alginate films obtained by
418 thermo-mechanical mixing, Food Hydrocolloids 63 (2017) 414-420.
419 [19] K. Xu, C. Liu, K. Kang, Z. Zheng, S. Wang, Z. Tang, W. Yang, Isolation of nanocrystalline
420 cellulose from rice straw and preparation of its biocomposites with chitosan: Physicochemical
421 characterization and evaluation of interfacial compatibility, Compos. Sci. Technol. 154 (2018) 8-17.
422 [20] D. Wang, W. Cheng, Q. Wang, J. Zang, Y. Zhang, G. Han, Preparation of electrospun
423 chitosan/poly(ethylene oxide) composite nanofibers reinforced with cellulose nanocrystals: Structure,
424 morphology, and mechanical behavior, Compos. Sci. Technol. 182 (2019) 107774.
425 [21] F. Chivrac, E. Pollet, M. Schmutz, L. Avérous, New approach to elaborate exfoliated
426 starch-based nanobiocomposites, Biomacromolecules 9(3) (2008) 896-900.
427 [22] F. Chivrac, E. Pollet, M. Schmutz, L. Avérous, Starch nano-biocomposites based on needle-like
428 sepiolite clays, Carbohydr. Polym. 80(1) (2010) 145-153.
429 [23] L. Meng, F. Xie, B. Zhang, D.K. Wang, L. Yu, Natural Biopolymer Alloys with Superior
430 Mechanical Properties, ACS Sustainable Chem. Eng. 7(2) (2019) 2792-2802.

[24] P. Chen, F. Xie, F. Tang, T. McNally, Competing interactions in dual-biopolymer nanocomposites, Compos. Sci. Technol. (2019) Submitted.

[25] J. Song, C. Chen, S. Zhu, M. Zhu, J. Dai, U. Ray, Y. Li, Y. Kuang, Y. Li, N. Quispe, Y. Yao, A. Gong, U.H. Leiste, H.A. Bruck, J.Y. Zhu, A. Vellore, H. Li, M.L. Minus, Z. Jia, A. Martini, T. Li, L. Hu, Processing bulk natural wood into a high-performance structural material, Nature 554 (2018) 224.

[26] M. Frey, D. Widner, J.S. Segmehl, K. Casdorff, T. Keplinger, I. Burgert, Delignified and Densified Cellulose Bulk Materials with Excellent Tensile Properties for Sustainable Engineering, ACS Appl. Mater. Interfaces 10(5) (2018) 5030-5037.

[27] F. Xie, T. Zhang, P. Bryant, V. Kurusingal, J.M. Colwell, B. Laycock, Degradation and stabilization of polyurethane elastomers, Prog. Polym. Sci. 90 (2019) 211-268.

[28] S. Sinha Ray, M. Okamoto, Polymer/layered silicate nanocomposites: a review from preparation to processing, Prog. Polym. Sci. 28(11) (2003) 1539-1641.

[29] M. Darder, M. López-Blanco, P. Aranda, A.J. Aznar, J. Bravo, E. Ruiz-Hitzky, Microfibrous Chitosan−Sepiolite Nanocomposites, Chem. Mater. 18(6) (2006) 1602-1610.

[30] M. Darder, M. Colilla, E. Ruiz-Hitzky, Biopolymer−Clay Nanocomposites Based on Chitosan Intercalated in Montmorillonite, Chem. Mater. 15(20) (2003) 3774-3780.

[31] F.S. Kittur, A.B. Vishu Kumar, R.N. Tharanathan, Low molecular weight chitosans—preparation by depolymerization with Aspergillus niger pectinase, and characterization, Carbohydr. Res. 338(12) (2003) 1283-1290.

451 [32] M. Matet, M.-C. Heuzey, E. Pollet, A. Ajji, L. Avérous, Innovative thermoplastic chitosan
452 obtained by thermo-mechanical mixing with polyol plasticizers, Carbohydr. Polym. 95(1) (2013)
453 241-251.
454 [33] H. Zhang, J. Wu, J. Zhang, J. He, 1-Allyl-3-methylimidazolium chloride room temperature ionic
455 liquid: A new and powerful nonderivatizing solvent for cellulose, Macromolecules 38(20) (2005)
456 8272-8277.
457 [34] J. Han, C. Zhou, A.D. French, G. Han, Q. Wu, Characterization of cellulose II nanoparticles
458 regenerated from 1-butyl-3-methylimidazolium chloride, Carbohydr. Polym. 94(2) (2013) 773-781.
459 [35] X. Tan, L. Chen, X. Li, F. Xie, Effect of anti-solvents on the characteristics of regenerated
460 cellulose from 1-ethyl-3-methylimidazolium acetate ionic liquid, Int. J. Biol. Macromol. 124 (2019)
461 314-320.
462 [36] S.-L. Quan, S.-G. Kang, I.-J. Chin, Characterization of cellulose fibers electrospun using ionic
463 liquid, Cellulose 17(2) (2010) 223-230.
464 [37] R.K. Layek, A. Kundu, A.K. Nandi, High-Performance Nanocomposites of Sodium
465 Carboxymethylcellulose and Graphene Oxide, Macromol. Mater. Eng. 298(11) (2013) 1166-1175.
466 [38] K. Shahzadi, I. Mohsin, L. Wu, X. Ge, Y. Jiang, H. Li, X. Mu, Bio-Based Artificial Nacre with
467 Excellent Mechanical and Barrier Properties Realized by a Facile In Situ Reduction and
468 Cross-Linking Reaction, ACS Nano 11(1) (2017) 325-334.
469 [39] N. El Miri, K. Abdelouahdi, A. Barakat, M. Zahouily, A. Fihri, A. Solhy, M. El Achaby,
470 Bio-nanocomposite films reinforced with cellulose nanocrystals: Rheology of film-forming solutions,

471 transparency, water vapor barrier and tensile properties of films, Carbohydr. Polym. 129(0) (2015)
472 156-167.
473 [40] C. Rosca, M.I. Popa, G. Lisa, G.C. Chitanu, Interaction of chitosan with natural or synthetic
474 anionic polyelectrolytes. 1. The chitosan–carboxymethylcellulose complex, Carbohydr. Polym. 62(1)
475 (2005) 35-41.
476 [41] N.M. Jennett, A.J. Bushby, Adaptive Protocol for Robust Estimates of Coatings Properties by
477 Nanoindentation, MRS Proceedings 695 (2001) L3.1.1.
478 [42] B.J. Briscoe, L. Fiori, E. Pelillo, Nano-indentation of polymeric surfaces, J. Phys. D: Appl. Phys.
479 31(19) (1998) 2395-2405.
480 [43] I. Quijada-Garrido, B. Laterza, J.M. Mazón-Arechederra, J.M. Barrales-Rienda, Characteristic
481 Features of Chitosan/Glycerol Blends Dynamics, Macromol. Chem. Phys. 207(19) (2006)
482 1742-1751.
483 [44] I. Quijada-Garrido, V. Iglesias-González, J.M. Mazón-Arechederra, J.M. Barrales-Rienda, The
484 role played by the interactions of small molecules with chitosan and their transition temperatures.
485 Glass-forming liquids: 1,2,3-Propantriol (glycerol), Carbohydr. Polym. 68(1) (2007) 173-186.
486

Highlights:

- ✓ Composites of chitosan/carboxymethyl cellulose (CMC)/nanoclay prepared
- ✓ Thermomechanical processing led to polyelectrolyte complexation between chitosan and CMC
- ✓ Chitosan/CMC films were more hydrolytically stable than chitosan-alone films
- ✓ Chitosan/CMC films had higher surface hydrophilicity than chitosan-alone films
- ✓ Chitosan/CMC complexed materials are potential for biomedical applications

Declaration of Interest

Thermomechanical-induced polyelectrolyte complexation between chitosan and carboxymethyl cellulose enabling unexpected hydrolytic stability

Pei Chen [a,b], Fengwei Xie [b,c,*,†], Fengzai Tang [d], Tony McNally [b,**]

[a] *College of Food Science, South China Agricultural University, Guangzhou, Guangdong 510642, China*

[b] *International Institute for Nanocomposites Manufacturing (IINM), WMG, University of Warwick, Coventry CV4 7AL, United Kingdom*

[c] *School of Chemical Engineering, The University of Queensland, Brisbane, Qld 4072, Australia*

[d] *WMG, University of Warwick, Coventry CV4 7AL, United Kingdom*

We wish to confirm that there are no known conflicts of interest associated with this publication.